

1-2018

Effects of Protein-Coated Nanofibers on Conformation of Gingival Fibroblast Spheroids: Potential Utility for Connective Tissue Regeneration

Gili Kaufman

Ryan A. Whitescarver


Laiz Nunes

Xavier-Lewis Palmer
Old Dominion University

Drago Skrtic

See next page for additional authors

Follow this and additional works at: https://digitalcommons.odu.edu/engtech_fac_pubs

 Part of the [Biomaterials Commons](#), [Biomedical Commons](#), and the [Materials Science and Engineering Commons](#)

Repository Citation

Kaufman, Gili; Whitescarver, Ryan A.; Nunes, Laiz; Palmer, Xavier-Lewis; Skrtic, Drago; and Tutak, Wojtek, "Effects of Protein-Coated Nanofibers on Conformation of Gingival Fibroblast Spheroids: Potential Utility for Connective Tissue Regeneration" (2018). *Engineering Technology Faculty Publications*. 63.
https://digitalcommons.odu.edu/engtech_fac_pubs/63

Original Publication Citation

Kaufman, G., Whitescarver, R. A., Nunes, L., Palmer, X. L., Skrtic, D., & Tutak, W. (2018). Effects of protein-coated nanofibers on conformation of gingival fibroblast spheroids: Potential utility for connective tissue regeneration. *Biomedical Materials*, 13(2), 025006. doi:10.1088/1748-605X/aa91d9

Authors

Gili Kaufman, Ryan A. Whitescarver, Laiz Nunes, Xavier-Lewis Palmer, Drago Skrtic, and Wojtek Tutak

Biomedical Materials



PAPER



Effects of protein-coated nanofibers on conformation of gingival fibroblast spheroids: potential utility for connective tissue regeneration

RECEIVED
13 April 2017

REVISED
26 September 2017

ACCEPTED FOR PUBLICATION
9 October 2017

PUBLISHED
24 January 2018

Gili Kaufman¹ , Ryan A Whitescarver¹, Laiz Nunes¹, Xavier-Lewis Palmer² , Drago Skrtic¹ and Wojtek Tutak³

¹ Volpe Research Center, American Dental Association Foundation, Gaithersburg, MD 20899, United States of America

² Department of Engineering and Technology, Old Dominion University, Norfolk, VA 23529, United States of America

³ Food and Drug Administration, Silver Spring, MD 20993, United States of America

E-mail: gili.kaufman@nist.gov

Keywords: collagen, fibrin, gingival fibroblasts, protein-coated nanofibers, spheroids, g-brush

Abstract

Deep wounds in the gingiva caused by trauma or surgery require a rapid and robust healing of connective tissues. We propose utilizing gas-brushed nanofibers coated with collagen and fibrin for that purpose. Our hypotheses are that protein-coated nanofibers will: (i) attract and mobilize cells in various spatial orientations, and (ii) regulate the expression levels of specific extracellular matrix (ECM)-associated proteins, determining the initial conformational nature of dense and soft connective tissues. Gingival fibroblast monolayers and 3D spheroids were cultured on ECM substrate and covered with gas-blown poly-(DL-lactide-co-glycolide) (PLGA) nanofibers (uncoated/coated with collagen and fibrin). Cell attraction and rearrangement was followed by F-actin staining and confocal microscopy. Thicknesses of the cell layers, developed within the nanofibers, were quantified by ImageJ software. The expression of collagen1 α 1 chain (Col1 α 1), fibronectin, and metalloproteinase 2 (MMP2) encoding genes was determined by quantitative reverse transcription analysis. Collagen- and fibrin-coated nanofibers induced cell migration toward fibers and supported cellular growth within the scaffolds. Both proteins affected the spatial rearrangement of fibroblasts by favoring packed cell clusters or intermittent cell spreading. These cell arrangements resembled the structural characteristic of dense and soft connective tissues, respectively. Within three days of incubation, fibroblast spheroids interacted with the fibers, and grew robustly by increasing their thickness compared to monolayers. While the ECM key components, such as fibronectin and MMP2 encoding genes, were expressed in both protein groups, Col1 α 1 was predominantly expressed in bundled fibroblasts grown on collagen fibers. This enhanced expression of collagen1 is typical for dense connective tissue. Based on results of this study, our gas-blown, collagen- and fibrin-coated PLGA nanofibers are viable candidates for engineering soft and dense connective tissues with the required structural characteristics and functions needed for wound healing applications. Rapid regeneration of these layers should enhance healing of open wounds in a harsh oral environment.

Abbreviations

ADAF	American Dental Association Foundation	Col1 α 1	collagen1 pro-alpha-1 chain
ANOVA	analysis of variance	cDNA	complementary deoxyribonucleic acid
COL1A1	collagen type I alpha-1 chain precursor	DI	de-ionized
		DMA	dynamic mechanical analysis

DMEM	Dulbecco's modified eagle medium
DPBS	Dulbecco's phosphate-buffered saline
ECM	extracellular matrix
EDTA	ethylenediaminetetraacetic acid
FBS	fetal bovine serum
GAPDH	glyceraldehyde 3-phosphate dehydrogenase
g-brush	gas-brush
LASAF	Leica application suite advanced fluorescence
LCSM	laser-scanning confocal microscope
M-ECM	Matrigel extracellular matrix
MMP2	matrix metalloproteinase 2
OD	optical density
PLGA	poly(DL-lactide-co-glycolide)
RNA	ribonucleic acid
RT-PCR	reverse transcription polymerase chain reaction
SD	standard deviation
SEM	scanning electron microscope
SV40LT	SV40 large T antigen
TCPS	tissue culture polystyrene

1. Introduction

Reconstruction of the masticatory mucosa, i.e. gingiva and hard palate, is required for closure of open wounds caused by trauma or surgery. Bacterial biofilms, microbial recolonization, and mechanical (mastication) forces existing in oral milieu are a constant challenge to the wound healing [1, 2]. Rapid regeneration of native mucosa is particularly important [3], since its connective tissues host the immune cells [4], and contribute to the alveolar bone modeling [5] and development of the epithelial layer [6, 7]. Gingival connective tissues (*lamina propria*) entail (i) loose, papillary thin layer, and (ii) a dense, thick reticular layer. The areolar connective tissue consists of a loosely arranged fiber network (including collagens) and cells. Fibroblasts support the epithelium by conveying oxygen and nutrients and permitting independent movement of inflammatory cells and mediators. Dense connective tissue is predominantly composed

of fibroblasts packed by collagen1 and fibrils that provide mechanical support and firm attachment for the other tissues and organs [8]. Culturing mucosal cell cultures on porcine skin or human cadaver dermis as a platform for engineered mucosa [9–11] does not involve fibroblasts, and long-term regeneration is unattainable. Oral mucosa grafting equivalent, which involves an acellular allogenic dermal matrix, was found to be more successful. This approach relies on the use of heterogeneous tissues, which again questions its long-term success. The major disadvantages of harvesting oral mucosa are its limited supply in the oral cavity and marked pain at the donor site [12].

Collagen, a principal component of the extracellular matrix (ECM), has a structural role in binding and reconnecting cell surface receptors, and a regulatory function through the engagement and activation of the specific cellular receptors [13]. Fibroblasts, one of the first responders in wounded tissues, interact with and attach to collagen primarily through their integrin receptors $\alpha2\beta1$, $\alpha1\beta1$, $\alpha11\beta1$ and $\alpha_v\beta3$. Other adhesion mechanisms rely on the 3D character of the matrix. In these 3D structures, the individual fibroblasts are tightly arranged between the collagen fibrils with varying diameters to achieve an optimal packing density [14]. Fibrin starts the activation and migration of various cell types including fibroblasts into the supportive matrix during wound healing [15, 16]. Fibrin also allows cells, such as fibroblasts, to spread more avidly on its monomers layers. $\beta1$ -subclass integrin is preferentially involved in the adhesion of fibroblasts to the RGD-segment monomers, due to a conformational change upon contact with its authentic vitronectin receptor $\alpha_v\beta_3$. Resultantly, $\beta1$ - $\alpha_v\beta_3$ complex is mobilized on the surface of fibroblasts upon contact with fibrin monomer monolayers [17, 18].

The main advantage of using 3D cell aggregates/spheroids in tissue regeneration is their ability to mimic not only the architecture of the cells *in vivo*, but also the cells' natural tendency to fuse and form tissue units with well-defined morphogenic and functional properties [19]. Tissue fusion is well documented throughout the embryonic development, and considered an essential step in cell rearrangement and sorting [20]. Spheroids are self-assembled macroscopic cell clusters, and their sizes are typically limited by the physics of gas and nutrients diffusion required to support their metabolic activity. Spheroids are typically considered scaffold-free micro-tissues that do not require biomaterials for their growth, support, or porosity, since they generate and organize their own 3D ECM [21, 22].

Nano- and sub-micron size polymer fibers are known for high aspect ratio, large surface-to-volume ratio, ECM-like morphology and inherently high bulk porosity [23]. Owing to those characteristics, these bio-mimetic materials allow for cell attachment, ingrowth, migration, differentiation and integration

[24]. However, polymer fibers alone have limited biological function due to lack of cell recognizable biomolecules [25, 26]. Therefore, presence of functional proteins on polymer surface is seen as a prerequisite for successful material integration with a host body. Protein coating on polymer devices can be achieved in variety of ways, including physio-sorption or chemical bonding [27, 28]. Physio-sorption allows for limited protein retention and cell interactions, and can be achieved by a simple ‘dipping’ process.

Functional protein layer/coat on polymer materials greatly enhances cell bioactivity and ability to form large cell structures [29]. To support skin and gingival tissue regeneration, materials would need to provide the most biologically relevant environment while providing gas diffusion, bio-mimetic morphology, structural integrity [30, 31], and flexibility to adapt to wound contours and protect from external liquids and mechanical forces [32]. Therefore, nanofiber scaffolds with a unique ability to diffuse nutrient/gas while providing bio-mimetic environment [29, 33] would make an excellent candidate for wound dressing applications.

Recently, our group has demonstrated that ECM-adhered gingival fibroblast monolayers and spheroids indeed migrate, rearrange, and create 3D cell-constructs. Covered with a thin layer of collagen hydrogel, these cells form large fused micro-tissues [22]. However, our scaffolds were not optimized for the reconstruction of gingival connective tissue—which requires a stiffer framework, that guides cells to organize and grow into multiple sequential cell layers. In this study, we have extended our 3D platform to gas-brushed (g-brushed) nanofiber scaffolds coated with physiologically relevant proteins intended for wound healing applications. Protein coating employed methodology similar to the material ‘dipping’ typically used to fabricate protein spun-blown fibers.

The underlying working hypotheses were: (1) covering the ECM-adhered gingival fibroblasts with protein-coated fibers will guide cell/spheroid migration and rearrangement into organized cell layers, thus mimicking their conformation in connective tissues, and (2) scaffolds will regulate/induce the expression of major ECM proteins and remodeling enzymes.

2. Materials and methods

2.1. Fiber and protein deposition by gas-blowing

The g-brush design entailed two air gas co-centric brushes operating simultaneously, as described previously [29] (figures 1(a), (b)). Polymer and protein suspensions were deposited by two syringe pumps (NE 1000 X, New Era System Inc., Farmingdale, NY) at a feed rate of 10–12 ml h⁻¹. A gas flow of approx. 5 l min⁻¹ was maintained during each g-brush operation. Gas pressure was measured using an USG® pressure gauge (pressure range: (0–1379) kPa)

mounted on a ‘Victor’ gas regulator. Omega FL-203a flow meter (model# FR4A40BVBVN-OM) was used to monitor gas flow.

2.2. Fabrication of polymer fiber scaffolds (mats)

A 75:25 poly-(DL-lactide-co-glycolide) (PLGA) (inherent viscosity (0.55–0.75) dL/g (Durect Corp., Birmingham, AL) was dissolved in ethylene acetate (Sigma-Aldrich, St Louis, MO) to achieve a 12 mass % PLGA solution. The solution was then fed to the g-brushes and fibers were gas-blown on a collector (figure 1(C)).

2.3. Preparation of protein solutions

Collagen1 and fibrin solutions were prepared according to modified manufacturer instructions. To make collagen1 solution, 15 μ l of 1 M NaOH solution was added to 100 μ l of 4 mg ml⁻¹ of rat-tail collagen type 1 (Advanced Biomatrix, San Diego, CA), mixed, and added to 800 μ l of fresh medium. Fibrin solution was made by mixing 150 μ l of fibrinogen with 1.5 μ l of 12 U ml⁻¹ of thrombin, and then added to a 3.0 ml media.

2.4. Fiber collection and cell culture specimen preparation

Polymer fibers were collected on a fiberglass or Teflon mesh positioned 15 cm to 20 cm away from the tip of the nozzle. After deposition, the scaffolds were removed (peeled off with use of tweezers), and cut with scissors into specimens for morphological analysis, mechanical testing, gas diffusion and cell culture tests (sections 2.5–2.11).

For cell culture studies, the nanofiber sections were placed over 12 mm tissue culture polystyrene (TCPS) discs, heat sealed around the edges, and stored in a desiccator under vacuum for later use. The discs were hot-punched from the bottom of TCPS petri dishes (100 mm diameter). Prior to use for cell cultures, the scaffolds were exposed for 3 min to ultraviolet germicidal irradiation, to inactivate microbiological contaminants during the gas-blowing. The disks were then mounted in a 48-well cell culture plate using Dow Corning® high vacuum grease (Dow Corning® Corp., Washington, DC), and washed with Dulbecco’s phosphate-buffered saline without calcium and magnesium (DPBS) (Life Technologies, Grand Island, NY).

2.5. Scanning electron microscopy (SEM) imaging

PLGA nanofibers were cut (with use of scissors) into 2 mm \times 5 mm pieces, mounted onto SEM stubs using carbon tape (Ted Pella, Inc., Redding, CA), placed under house vacuum and desiccated overnight. Specimens were sputtered (120 s at 75 mA, Desk V HP; Denton Vacuum, Moorestown, NJ) with approximately 10 nm of gold. Six SEM images—three at high (13 000x or 15 000x) and three at low magnification

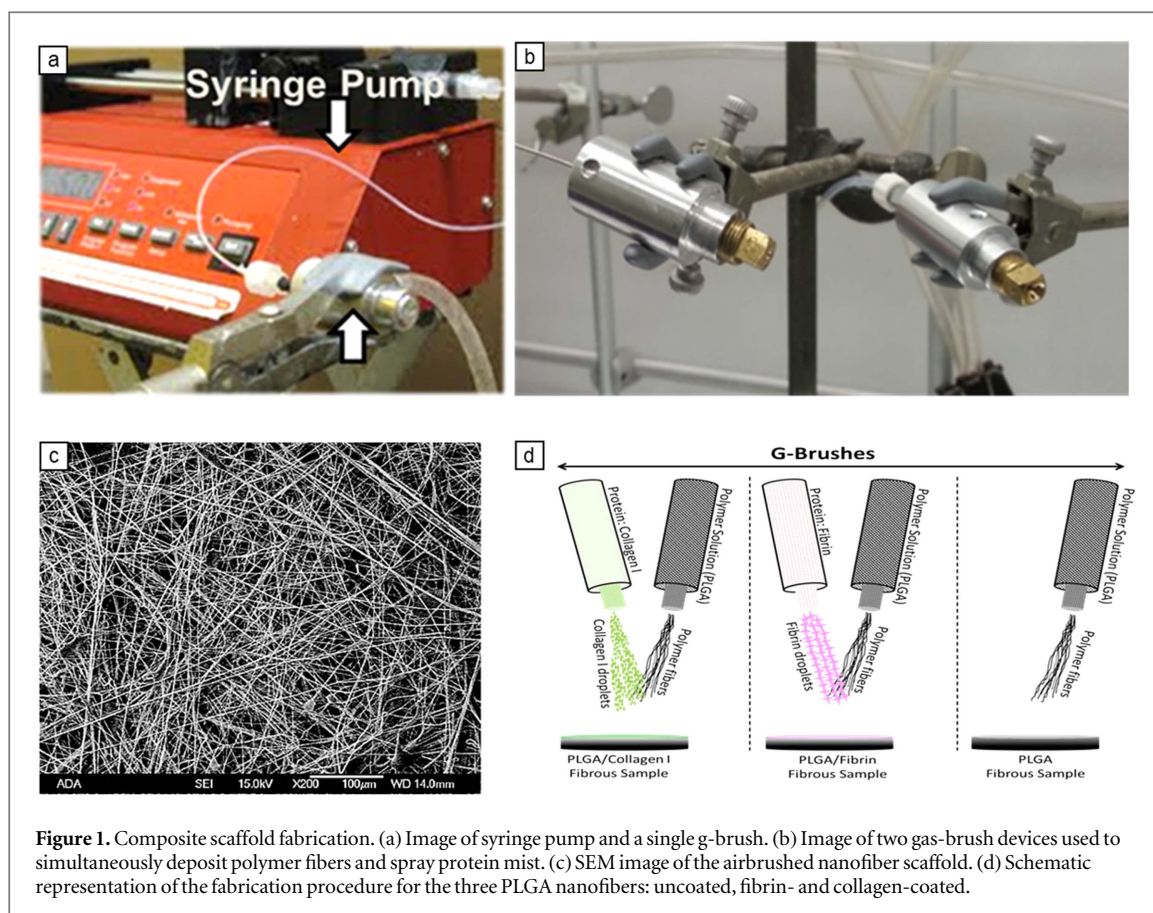


Figure 1. Composite scaffold fabrication. (a) Image of syringe pump and a single g-brush. (b) Image of two gas-brush devices used to simultaneously deposit polymer fibers and spray protein mist. (c) SEM image of the airbrushed nanofiber scaffold. (d) Schematic representation of the fabrication procedure for the three PLGA nanofibers: uncoated, fibrin- and collagen-coated.

(500x)—were captured of each sample (3 kV, 7 mA, ≈ 13 mm working distance; Hitachi S4700, Hitachi America, Tarrytown, NY). Excel-exported data were analyzed by OriginPro © software (OriginLab; Northampton, MA).

2.6. Nanofiber diameter assessment

The morphology of the PLGA nanofibers was assessed as outlined in [29]. An ImageJ plugin [30], called DiameterJ, created by Dr Nathan Hotaling, was used to calculate nanofiber diameter and other parameters. The plugin works through a two-step process entailing the binary image segmentation of a micrograph, followed by analysis [34]. Image segmentation employs thresholding techniques within ImageJ and segmentation algorithms developed independently, followed by refining algorithms for noise reduction and morphological smoothing. This plugin has been validated *in silico* from more than 130 digital image sets and SEM images of diametrically defined wires—in addition to expanding use in publications since its release in 2015. Fiber diameter was calculated from $n \geq 20\,000$ measurements via superpixel determination [34], which essentially divides the total fiber area by the total length of the fiber centerlines. The characteristic length, i.e. the mean fiber length between the intersections, was calculated by dividing the centerline length of the fibers by the number of intersections.

2.7. Mechanical testing

Tensile tests were performed using a Dynamic Mechanical Analysis (DMA RSA3; T.A. Instruments, New Castle, DE) with fiber/film tools installed. Samples ($n \geq 3$) were 2 cm long, 1 cm wide, and 200 μm to 300 μm thick. A constant elongation rate of 0.2 mm min^{-1} was used, and the normal force transducer was set in the low range. Young's modulus was calculated from the stress/strain linear relationship existing in the low strain region (between 5% and 9%).

2.8. Coomassie blue staining

Cell culture scaffolds (collagen, fibrin and non-coated, $n = 3/\text{group}$) were stained with a coomassie stain (Sigma-Aldrich) for 30 min, and then rinsed three times with PBS and de-ionized (DI) water, until no traces of dye were detected in non-coated controls. The light microscope images were then taken, and the results were compared.

2.9. Filter integrity test/gas diffusion test

Filter integrity test unit (Sartorius Stedim biotech Sartocheck® 4 Plus, 2014 model, Bohemia, NY, USA) was employed to test air diffusion rate through non-coated and protein-coated scaffolds. Scaffolds were deposited and cleaned as described earlier in section 2.4. To fit the scaffolds into a sample holder (membrane adapter), they were cut into 47 mm diameter discs with an average of approximately 1 mm thickness. A minimum of four membranes was tested

in each experimental group. Measurements were performed by following the manufacturer's protocol.

2.10. Fibroblast cell cultures: monolayer and spheroids

SV40LT immortalized mouse gingival fibroblasts (ESK-1; a generous gift from Dr John R Klein from the University of Texas Health Science Center) were cultured in Dulbecco Modified Eagle Medium (DMEM) supplemented with 10% fetal bovine serum (FBS), 2 mM L-glutamine, 100 units ml⁻¹ of penicillin and 100 µg ml⁻¹ of streptomycin (Invitrogen, San Diego, CA). At 80% confluence, cells were split at 1:50 ratios and then plated on 48-well plates (Greiner bio-one; Monroe, NC) to form spheroids. 3D cell cultures were prepared by coating the 48-well plate surfaces with 100 µl MatrigelTM-ECM (M-ECM: Corning Life Sciences, Acton, MA), and incubating for 30 min; 0.17×10^5 cells were then seeded on the solidified M-ECM, and incubated for 2 h. The adherent cells were then covered with 10% M-ECM, and incubated for 14 days as described previously [22]. The mature fibroblast-spheroid cultures were washed twice with Dulbecco's phosphate-buffered saline (DPBS; Invitrogen), and incubated with Dispase (Corning Life Sciences) diluted 1:400 with DPBS. Next, the suspension was incubated for 2–3 h, and centrifuged at $340 \times g$ (Eppendorf centrifuge 5804R; Eppendorf, Hauppauge, NY). The dissociated spheroids were treated with 0.25% trypsin- ethylenediaminetetraacetic acid (EDTA; Invitrogen), and direct cell counts were taken by using hemocytometer (Hausser Scientific, Horsham, PA) after 0.4% trypan blue staining (Invitrogen). Equal numbers (1×10^5 cells) of fibroblasts in monolayers and spheroids were seeded on the M-ECM coated 24 well plate (Greiner bio-one), and incubated for 2–3 h to enable cell adhesion. The following cell amount was demonstrated to be sufficient for the development of a full-thickness human oral mucosal equivalent [3, 35, 36]. Collagen1- and fibrin-coated nanofiber disks were placed on top of the cell cultures, to enable cell-fiber interactions. The uncoated PLGA nanofibers were used as a negative control group, and collagen1 and fibrin hydrogels [22] were used as positive controls. The wells were filled with 500 µl of the fresh medium, and incubated for 14 d. Cell cultures were incubated in an Air-Jacketed Automatic CO₂ Incubator (NuAire, Plymouth, MN) at 37 °C and 5% CO₂. Culture media were replenished twice a week.

2.11. Cell staining, imaging and image analysis

The samples (gingival fibroblasts and their derived spheroids) were detached gently from the ECM surface, washed twice with DPBS, fixed with 4% paraformaldehyde (Electron Microscopy Sciences, Hatfield, PA), and permeabilized for 5 min with 0.1% Triton X-100 (Alfa Aesar, Ward Hill, MA). Cells' F-actin was

stained with 0.1 mM phalloidin for 30 min (Molecular Probes, Eugene, OR). Finally, the samples were washed twice, and kept in DPBS at 4 °C before being analyzed. The autofluorescence of the coated and uncoated PLGA fibers was visualized by using the FITC channel at 490 nm, as described previously [37].

Phase contrast images of the fibroblast-spheroid cultures covered by nanofibers were taken by stitching sliced images along the *z*-axis (motorized inverted Eclipse Ti-E epifluorescence microscope; Nikon Instruments Inc., Melville, NY) using the NIS-Elements software version 3.0 (Nikon Instruments Inc.). Images of the fibroblasts/PLGA scaffolds were collected using a laser-scanning confocal microscope (LCSM; Leica Microsystems Inc., Buffalo Grove, IL) with two fluorescence channels and ~3.5 µm nominal optical slice thickness. Approximate sample dimensions were measured along *x*–*z* and *y*–*z* planes using Leica Application Suite Advanced Fluorescence (LASAF) software (Leica Microsystems Inc.). 3D sample projections were created by stacking the images (LCSM), and analyzed using ImageJ software (V.1.48, NIH).

2.12. Quantitative reverse transcription polymerase chain reaction (qRT-PCR) analysis

Total ribonucleic acid (RNA) was extracted directly from spheroids cultured in the nanofibers using the RNeasy Fibrous Tissue Mini Kit (Qiagen, Valencia, CA), and quantified using a Nanodrop ND-100 spectrophotometer (NanoDrop Technologies, Wilmington, DE). Complementary deoxyribonucleic acid (cDNA) was generated with SuperScript III cDNA first strand synthesis kit (Invitrogen; used according to the manufacturer's instructions), and its total yield quantified through optical density (OD) measurement. PCR analysis and Real-Time PCR measurements were carried out by using Platinum Taq DNA polymerase kit (Invitrogen) and SYBR Green PCR Master Mix (Applied Biosystems, Foster City, CA) according to the manufacturer's manual. The following oligonucleotides (Integrated DNA Technologies, Coralville, IA) were used for RT-PCR analysis to amplify the house-keeping gene: glyceraldehyde 3-phosphate dehydrogenase (GAPDH); extracellular matrix major supportive proteins: collagen1 (Col1α1) and fibronectin (Fibro); extracellular matrix turnover metalloproteinase: MMP2. GAPDH (forward:5'ggtcggtgtgaaggattt3'; reverse:5'gtggatgcaggatgatgtt3'); mouse Col1α1 (forward:5'gccagaagacatccctgaa3'; reverse:5'aggacatctgggaagcaag3'); mouse Fibro (forward:5'acggagagacaggaggaata3'; reverse:5'cagtgtgtccttgagacatag3'); mouse MMP2 (forward:5'gttcaacggtcgggaataca3'; reverse:5'tgtcactgtccgcaataa3'). For the Real-Time PCR analysis, the following oligonucleotides were used: GAPDH as an internal control (forward:5'aacagcaactcccactctt3'; reverse:5'cctgttctctagccgtatt3'), Col1α1 (forward:5'ccgctctgctcct

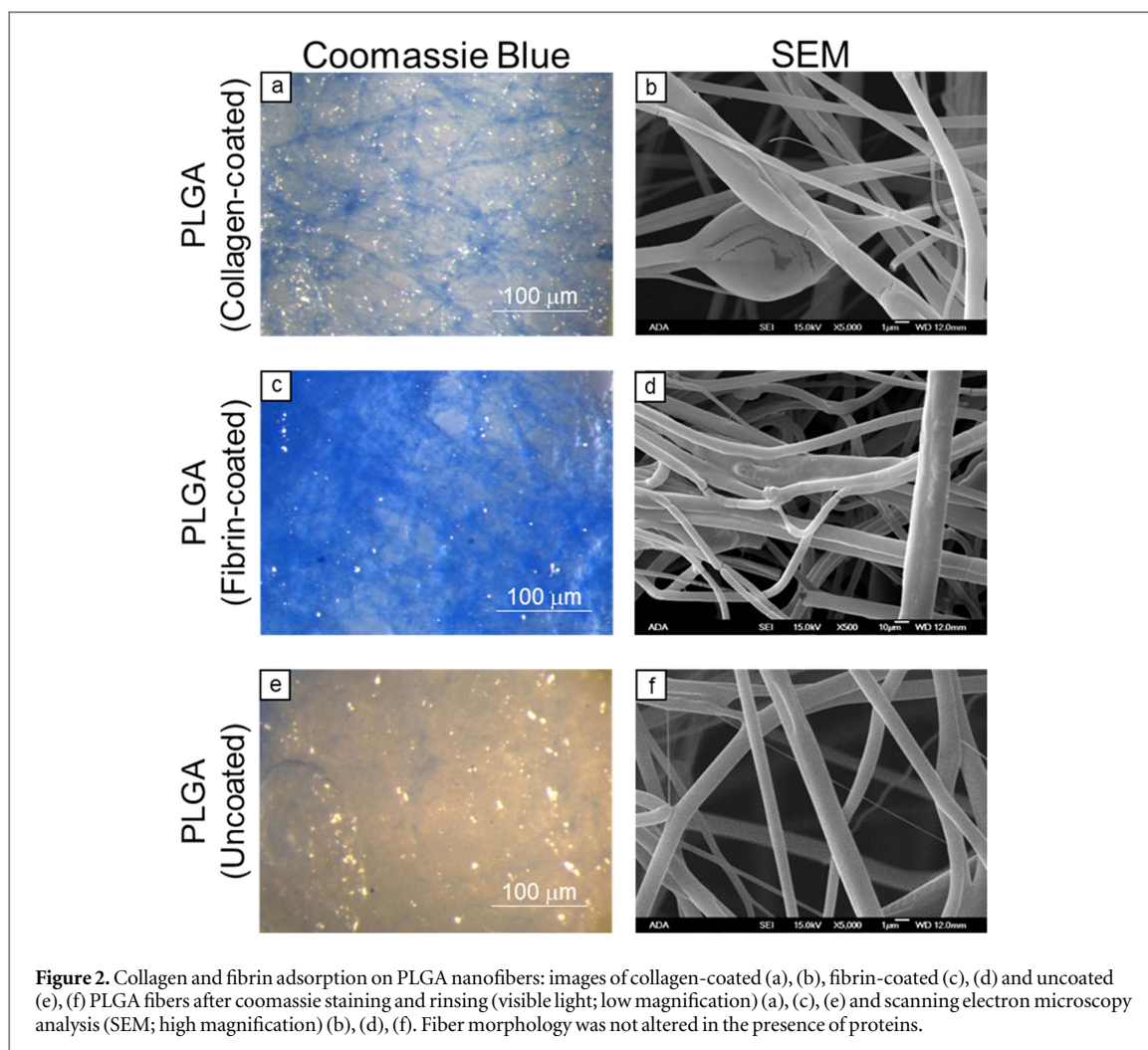


Figure 2. Collagen and fibrin adsorption on PLGA nanofibers: images of collagen-coated (a), (b), fibrin-coated (c), (d) and uncoated (e), (f) PLGA fibers after coomassie staining and rinsing (visible light; low magnification) (a), (c), (e) and scanning electron microscopy analysis (SEM; high magnification) (b), (d), (f). Fiber morphology was not altered in the presence of proteins.

tta3'; reverse: 5'cattgtgtatgcagctgacttc3') and Fibronectin (forward: 5'tgtgaccagcaacacgggtg3'; reverse: 5'acaacaggagagtagggcg3'). Integrity and equal loading of cDNA reactions were checked by quantification of GAPDH. RT-PCR and Real-Time PCR analysis were done using the SimplyAmp™ thermal cycler and Viia™ 7 Real-Time PCR System (Applied Biosystems), correspondingly. PCR analysis was repeated at least three times for every RNA sample.

2.13. Statistical analysis

A minimum of three replicates ($n \geq 3$) was analyzed for filter integrity/gas diffusion testing. Experiments entailing fibroblast cultures treated with collagen/fibrin PLGA nanofibers (coated and uncoated) and collagen/fibrin infused hydrogels were run in triplicate. Microscopic observations, thickness and growth area measurements were performed on 10-representative images/replicate/group. RT-PCR experiments/gene/experimental group were also performed in triplicate. Mean values and standard deviation (\pm SD) of the membrane thickness measurements were performed using one-way analysis of variance (ANOVA) followed by two-tailed Student's *t*-test for the unpaired samples. Results were considered

statistically significant when $p \leq 0.05$. Statistical analysis of the constructs thickness and boxplots were computed in 'R' (version 3.2.1).

3. Results

3.1. Synthesis and characterization of collagen- and fibrin-coated PLGA nanofibers

Combining a basic g-brush, and adding another brush (figures 1(a), (b)), enabled us to co-deposit biodegradable PLGA nanofibers (figure 1(c)) and proteins (figure 2) by employing technologies previously developed in our lab [38]. Polymer fibers deposited from the first g-brush were instantaneously covered with either type 1 collagen or fibrin (figure 2). Bulk properties of the 'neat' (protein-free) nanofibers are summarized in table 1. These fibers had an average diameter of (830.4 ± 532.3) nm, with an average length between the fiber intersections of (2.2 ± 1.1) μ m. The mats had an average pore size of (5.7 ± 1.1) μ m², calculated porosity (64.30 ± 11.01) % and they diffused on average $[(18.22 \pm 9.33)$ ml min⁻¹] of water at 1 Pa. Their elastic modulus was relatively low $[(1.98 \pm 0.61)$ MPa], ultimate strength (0.25 ± 0.10) MPa and the ultimate strain (13.7 ± 4.1) %.

Table 1. Bulk properties of protein-free nanofibers^a.

Fiber diameter (nm)	830.4 ± 532.3
Characteristic length between fiber intersections (μm)	2.2 ± 1.1
Fore size (μm^2)	5.7 ± 1.1
Porosity (%)	64 ± 11
Water diffusion ^b (ml min^{-1})	18.2 ± 9.3
Elastic modulus (MPa)	2.0 ± 0.6
Ultimate strength (MPa)	0.26 ± 0.10
Ultimate strain (%)	13.7 ± 4.1

^a Indicated are mean values ± standard deviation (SD).

^b Mat thickness approx. 1 mm; 1 Pa of DI water.

The retention of the proteins on the material surface was verified by coomassie staining (figures 2(a), (c), (e)). After thorough rinsing with DI water, collagen and fibrin scaffolds stained blue (figures 2(a) and (c), respectively) contrary to the uncolored fibers in the control samples (PLGA fibers; figure 2(e)). SEM screening of collagen-, fibrin- and control scaffolds showed no morphological differences (figures 2(b), (d) and (f), respectively). The basic fibers had no visible polymer blubs/defects or extensive charging effect characteristic of the protein presence. The matrix bio-functionality was further verified by cell culturing as discussed below.

3.2. Fibroblasts migration and rearrangement within the nanofibers driven by coated proteins

Gingival fibroblasts plated on ECM surfaces, covered with either collagen or fibrin-coated nanofibers and cultured for three weeks are shown in figures 3(a)–(c) and figures 3(d)–(f) respectively. Cells migrated toward and within the scaffold and navigated to the inner layers of the fibers. Cell adhesion and surface penetration in uncoated fibers (PLGA control) was negligible compared to the coated ones (figures 3(g)–(i)). Cells migrated into the collagen fibers and formed densely clustered structures mostly along the planar surface of the fibers (figure 3(b)). However, fibroblasts grown on fibrin nanofibers were dispersed and formed larger intercellular intervals (figure 3(e)). The thickness of the cell layers cultured within collagen was significantly ($p \leq 0.001$) higher when compared to the cells exposed to the uncoated (control) nanofibers [(31.5 ± 8.5) μm versus (13.7 ± 3.0) μm respectively] (figures 3(c), (i), (j)). Apparently higher thickness of fibroblasts grown within the fibrin nanofibers compared to the control group was significantly different [(21.4 ± 9.1) μm versus (13.7 ± 3.0) μm ; $p \leq 0.01$; (figures 3(f) and (j))]. Difference in the thickness of cell layers in PLGA-collagen and PLGA-fibrin scaffolds was statistically significant ($p \leq 0.001$) (figure 3(j)). These results suggest that the cells responded to the fibrous matrix, and that their activity was enhanced by the presence of the proteins. In addition, the capability of monolayered fibroblasts to attach and penetrate the scaffolds

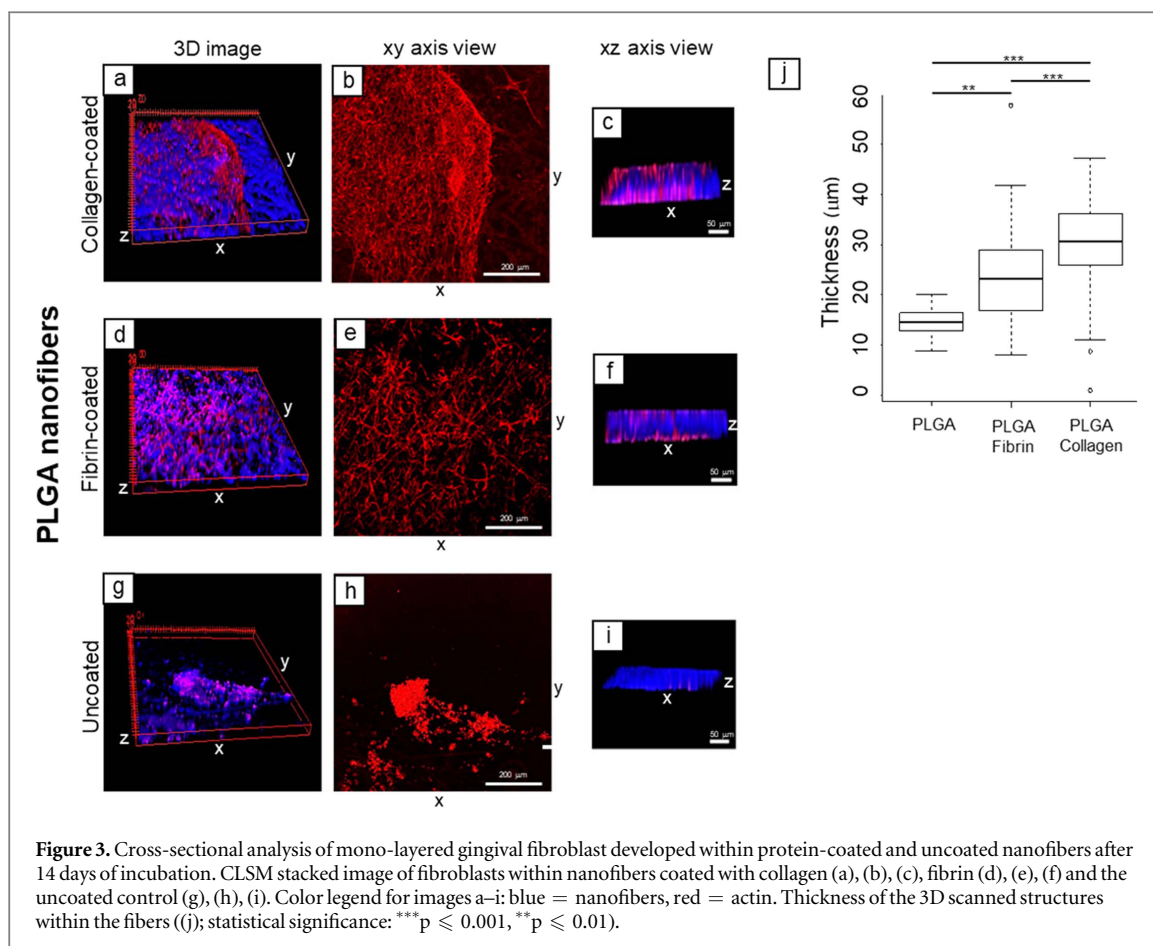
after three days of incubation was found to be negligible across the coated and uncoated scaffolds, and could barely be detected (data not shown).

3.3. Fibroblast spheroids enhance the thickness and rapid rearrangement of cell layers within the coated fibers

After 3 days of incubation, fibroblast spheroids integrated with both collagen (figure 4(a)) and fibrin (figure 4(b)) coated proteins by developed elongated cell extensions out of the spheroid structures (figures 4(a) and (b); pointed by the arrow). These features were not detected in cells covered with the uncoated fibers (figure 4(c)) or in M-ECM control group (figure 4(d)). Moreover, a dense conformation of the fibroblasts was maintained under collagen fibers while undergoing modification in fibrin group (figure 4(b)). Initial interactions of the extended cells with both collagen and fibrin nanofibers are illustrated in figures 4(e)–(g) and figures 4(h)–(j), respectively.

Fibroblast spheroids formed in collagen scaffolds continued expressing a compact spatial arrangement after 14 days of incubation (figures 5(a), (b)). They occupied the entire 3D space of the scaffold (figure 5(c)), and fused into larger, continuous structures (figures 5(a), (b); fusion site indicated by the white arrow). On the other hand, the architecture of spheroids, grown within fibrin nanofibers, underwent modifications—cells were scattered, and allowed the formation of intercellular intervals (figures 5(d), (e)). These cells could not consistently grow across the entire section of the fibers layers (figure 5(f)), showed no fusion (figures 5(d), (e); gaps between the spheroids are pointed by the yellow arrow), and although attached to the uncoated fibers, these fibroblasts could not develop further into 3D constructs (figures 5(g)–(i)). The thickness of the cell layers increased significantly ($p \leq 0.001$) in collagen versus fibrin scaffolds [(86.1 ± 12.15) μm and (53.7 ± 17.5) μm respectively], and for both protein types was significantly ($p \leq 0.001$) higher than in their control scaffold counterparts [(13.4 ± 4.6) μm] (figure 5(j)).

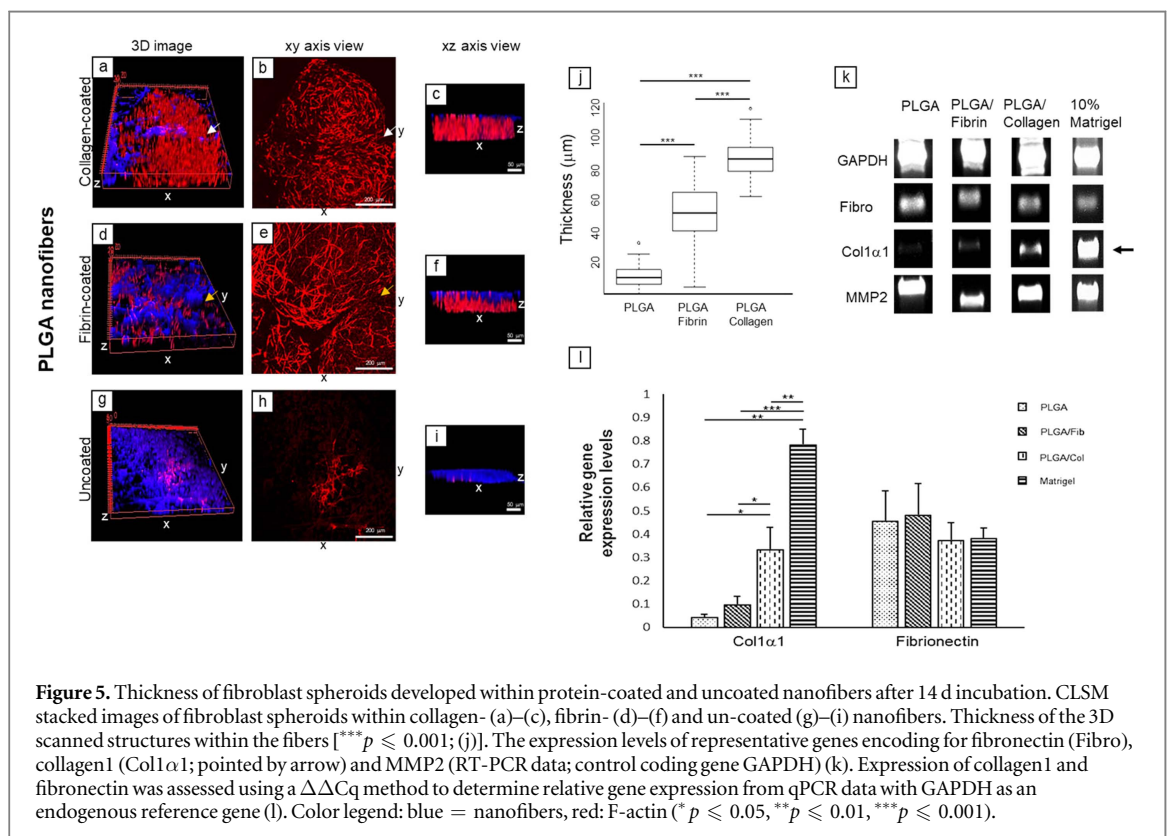
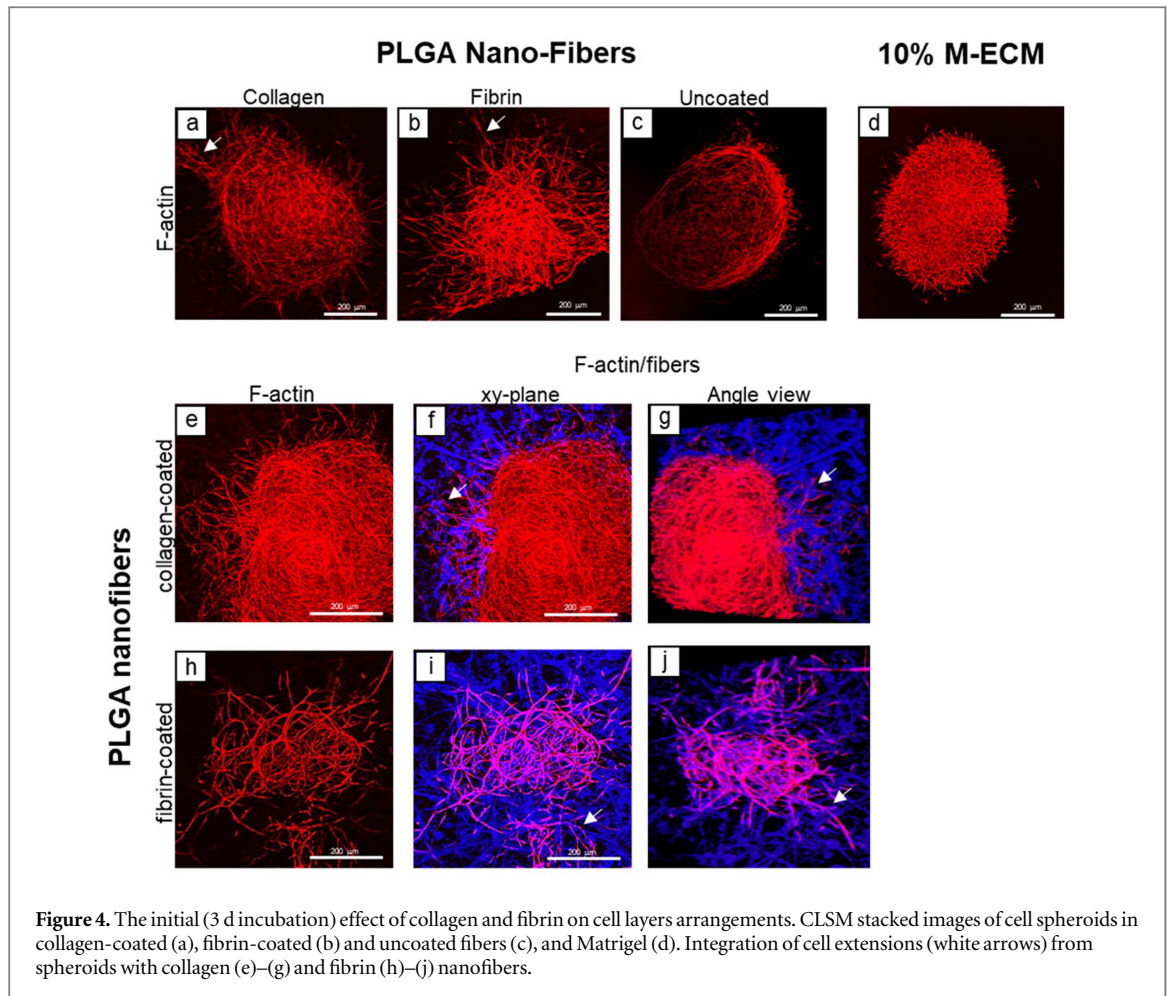
The quantitative RT-PCR analysis revealed elevated expression of the collagen1 major chain $\alpha 1$ (Col1 $\alpha 1$) gene in collagen nanofibers, compared to fibrin counterparts (figure 5(k); pointed by the arrow). In spheroids attached to collagen fibers, Col1 $\alpha 1$ expression was 3-fold and 9-fold higher ($p \leq 0.05$) compared to spheroids attached to fibrin and uncoated fibers, respectively. Cells attached to fibrin fibers also demonstrated 3-fold increase in their Col1 $\alpha 1$ expression compared to those attached to uncoated PLGA fibers (figure 5(l)), thus demonstrating high-level type 1 collagen synthesis and secretion by fibroblasts. The genes coding for fibronectin and MMP2 were expressed at constant levels in all experimental groups (figures 5(k), (l)).

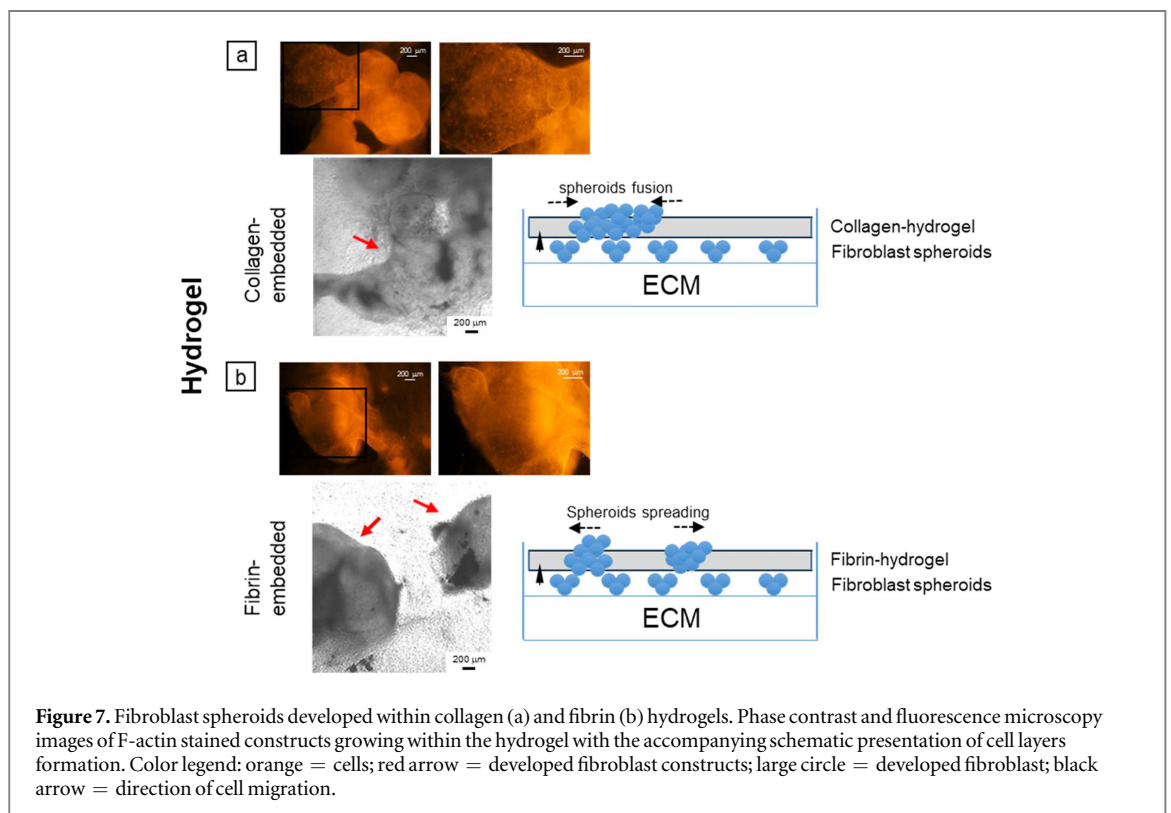
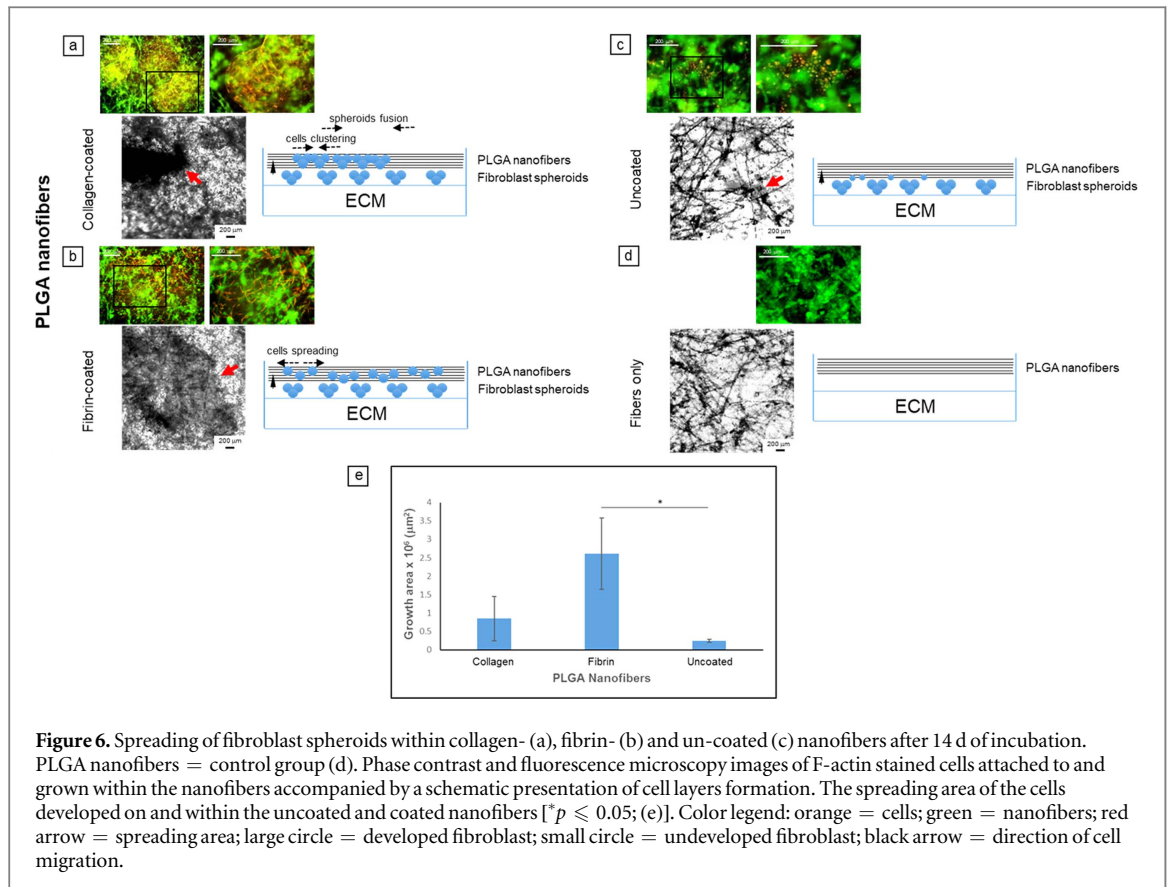


After 14 days of incubation, development of fibroblast constructs within collagen and fibrin nanofibers was remarkably different. Collagen retained the bundled cell rows and spheroidal structures ultimately supporting spheroid fusion (figure 6(a)). Fibrin disassembled the aggregated fibroblasts leading to widely dispersed cells with large intercellular gaps (figure 6(b)). Fibroblasts attached to the uncoated fibers changed morphology from elongated spindle-shaped cells into small circular ones (figure 6(c)). Compared to the uncoated fibers cultured without cells, nanofiber architecture remained apparently unaffected by cell attachment and growth (figure 6(d)). The growth area of fibroblasts within fibrin fibers [$(2.61 \pm 0.96 \times 10^6) \mu\text{m}^2$] was larger than the corresponding growth areas within collagen fibers [$(0.85 \pm 0.60 \times 10^6) \mu\text{m}^2$] and uncoated fibers [$(0.24 \pm 0.04 \times 10^6) \mu\text{m}^2$; $p \leq 0.05$]. Architectural differences were also seen between fibroblasts grown within collagen and/or fibrin-coated fibers compared to cells cultured in collagen and/or fibrin embedded hydrogels (figures 6(a), (b) versus 7(a), (b)). Cellular spatial growth and orientation within the fibers were more constrained to the fibers planar area compared to cells grown within hydrogels. Fibrin leads to the spread of fibroblast aggregates and individual cells in hydrogels and nanofibers (figures 6(b) and 7(b) respectively).

4. Discussion

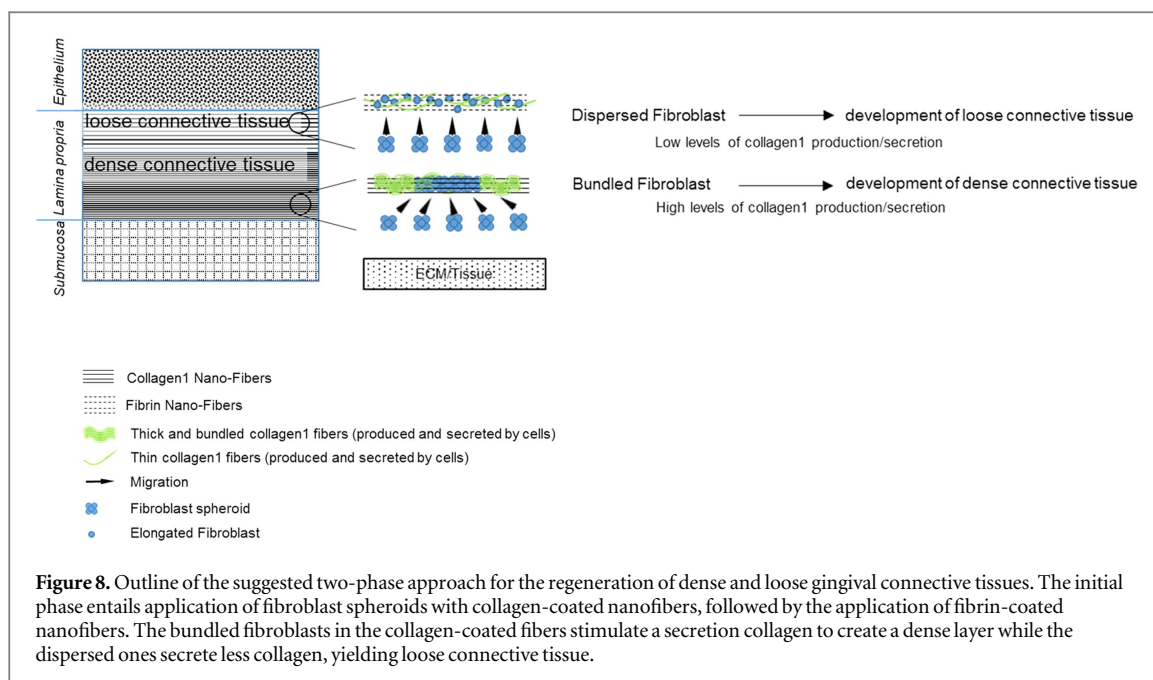
Bio-mimetic, nanostructured fibers are an attractive new type of material for tissue regeneration because they have similar sub-micron and micron morphology and dimensions (200–600 nm in diameter) as the native fibrous ECM matrix proteins, i.e. collagen and fibrin. Generally, bio-mimetic scaffolds support cell adhesion, proliferation and differentiation [29, 39, 40]. Bio-mimetic hydrogels, currently the most frequently used materials in tissue engineering, often fail to incorporate physical, chemical, temporal and spatial gradients within the engineered 3D scaffolds. Their drawbacks include poor oxygen/nutrient diffusion rates, inadequate morphology (short fibers in form of gel), relatively weak mechanical properties [42], and a wide range of elasticity (Young's modulus of 1–100 kPa [43]). The g-brushed bio-mimetic scaffolds evaluated in this study present a viable engineering alternative to traditional tissue regeneration. These scaffolds provide an environment that can support and guide tissue repair. G-brushed synthetic matrices discussed in this study with average diameter ~ 830 nm, calculated porosity of 64% and pore size of $5.7 \mu\text{m}^2$ have a collagen-like morphology and tissue-similar properties [44–46]. Typically, polymer fibers generated by either electrospinning or airbrushing exhibit a wide range of fiber diameters [34, 35, 47]. According to our experience, electrospun/airbrushed





fiber diameter typically varies between 30% and 80% of the reported medium/average, unless the fabrication is done in an environmentally controlled room. This finding correlates well with reports in the literature [34, 47]. The main contributing factors

influencing electrospun/airbrushed fiber diameter are: environment (humidity and temperature which both affect the solution evaporation rate), polymer/solvent properties, deposition rate and nozzle configuration [34, 35, 47, 48]. The effect of physio-sorbed



protein on fiber distribution is expected to be negligible (or nonexistent) due to the dominating effect of the environmental factors and polymer/solution properties on fiber diameter.

Since diffusion through a membrane or tissue is a very important factor in exchanging gas, liquids and nutrients needed to form/regenerate tissue, we have quantified this property of our scaffolds. An approx. 1 mm thick layer of PLGA nanofibers can initially diffuse approx. 18 ml min^{-1} of water, while providing pliable yet structurally robust scaffolds (Young's modulus of approx. 2 MPa; stretching-out up to 14% when pulled at approx. 0.3 MPa). For comparison, a typical Band-Aid is much more mechanically robust, but it cannot diffuse gas or be placed intraorally. On the other hand, typically low water permeation rates and poor handling properties make hydrogels difficult to apply in wound dressings [49].

Synthetic polymers alone provide poor interaction platforms for cells and coating with protein enhances material–cell interactions, cell attraction, migration and spatial organization. Mixing proteins and polymer solution prior to their electro-deposition has already been explored in a ‘dipping’ process [39]. Such an approach was proven adequate to yield bio-functional protein-coated fibers. In this study, we used a modified version of the ‘dipping’ process by co-gas-brushing fibers and proteins. Our approach is easy to employ and, as suggested by our results, adequate to coat the fibers with proteins. The proteins deposited on the PLGA fibers are likely physio-sorbed onto surface where they stay in active form. These features were indirectly confirmed by coomassie staining, and verified in cell culture experiments. Fibroblasts recognized and reacted to the surface coatings; the extent of these interactions was protein-specific. In contrast, control-PLGA fibers supported cell growth without

allowing for larger cell structure formation. We believe that proteins, physio-sorbed and/or adsorbed onto fibers by weak van der Waals forces and/or ionic bonds, will have short stability in the liquid medium (detachment/replacement by present ions/small proteins) but relatively long stability in air [50]. After initial cell attachment to the fibers, proteins will be either remodeled by cells or replaced by other proteins/ions secreted by the cells to the media. Protein adsorption on the polymers followed by cell responses involve complex processes. For example, spray-dried PLGA micromolecules: (i) adsorb proteins at higher rate than macromolecules fabricated using other techniques, and (ii) absorb more proteins than other polymer types [51]. It has also been demonstrated that cells (e.g. HUVEC) prefer to adhere to hydrophilic surfaces coated with the adsorbed proteins [52]. Our results directly support these previously reported protein/fiber relationships, and yield enhanced cell-material interactions.

Collagen most closely replicates the conditions and the architecture in the dense connective tissue, where fibroblasts are tightly arranged in between the collagen fibrils [29]. During wound healing, fibroblasts initially migrate into the wound area to remodel the extracellular matrix by secreting components such as collagen [53]. In the final stages, collagen agglomerated to create the granulation tissue. ECM-adherent mono-layered cells are found to attract the collagen nanofibers [54]. They migrate and organize in a conformation that resembles clustered structures, which might be explained by the mobilizing effect of the integrin receptors family $\alpha_2\beta_1$, $\alpha_1\beta_1$, $\alpha_{11}\beta_1$ and $\alpha_v\beta_3$ [14]. Fibrin, which participates in the initial stage of the wound healing process, creates a network that attracts various cell types including fibroblasts to develop the clot [55]. However, cellular structural

rearrangement within the fibrin nanofibers contrasted with the conformations observed within collagen nanofibers. Various distributions of fibroblasts attached to uncoated, collagen- and fibrin-coated fibers resemble cell distributions reported in previous studies [39, 56]. The most important difference was the scattered fibroblasts that created intercellular intervals. These intervals resembled the structural architecture of interspersed embedded fibroblasts localized in loose connective tissue [45]. Fibroblast motility and arrangement along the fibrin may be explained by the mobilizing effect of the $\beta_1\text{-}\alpha_v\beta_3$ receptor complex present in fibrin proteins [17, 18]. Formation of the intercellular space allows the development of chemoattractant and mediator gradients that play an important role in the wound healing regulation process. The cell layers developed within the collagen nanofibers were apparently thicker than those developed within the fibrin nanofibers, and the differences between the two groups were statistically significant. It needs to be pointed out that the thicknesses of the layers within the collagen and fibrin fibers significantly exceeded the thickness of surface layers of the uncoated controls.

The motivation for employing gingival fibroblast spheroids instead of mono-layered cells is based on the findings of our previous study [22], i.e. a significant increase in the development and thickness of 3D fibroblast constructs when ECM-adherent fibroblasts spheroids were covered with collagen-blended hydrogels. In the current model, structural rearrangements were similar in both collagen and fibrin composite scaffolds. The thickness of the cell layers in both groups was above 50 μm . Cells that grew within the collagen nanofibers were approx. 2.5 times thicker than the cells in fibrin matrices. Furthermore, cell layer thickness was more consistent (with less variability) in collagen scaffolds compared to fibrin ones, because of the condensed cell structures existing in the collagen group. Fibroblast spheroids started interacting with the nanofibers after 3 d of incubation. In contrast, no mono-layered fibroblasts were detected attached to the fibers after the same time period. It is particularly important that this potential to interact early with proteins is detected not only in hydrogels but also in coated PLGA nanofibers. These fibers provide a firm, supportive framework that promotes structural development of cell layers into configurations that resemble the *in vivo* environment by guiding their homogeneous planar distribution. The thickness of the fibroblast-spheroid layers developed within the nanofibers was more than eight times smaller than the thickness of the layers obtained from growing within collagen1-embedded hydrogels, as we had described earlier [22].

The gene expression profiling revealed that structural proteins, such as collagen and fibronectin, and ECM turnover enzyme MMP2 were expressed in both protein groups. The expression of the major

component of type 1 collagen, i.e. its alpha-1 chain precursor (COL1A1) encoded by *col1 α 1* gene, was elevated significantly— three-fold—in fibroblast layers developed within collagen nanofibers, in comparison to those developed within fibrin nanofibers. However, collagen- and fibrin-coated fibers enhanced the expression of *col1 α 1* in the attached fibroblasts nine- and three-fold respectively, compared to the uncoated fiber. A decrease in the proliferation and metabolic activity of fibroblasts attached to collagen-coated fibers has recently been related to cells clustering via cell migration [39, 56]. This finding correlates well with the outcome of previous studies [57, 58]. Increased secretion of collagen1 is needed to engulf cells, and create a microenvironment resembling dense connective tissue. On the other hand, lower levels of collagen1 secretion in fibrin nanofibers resulted in cells with scattered architecture and intercellular compartments, a unique property of the loose connective tissues [54]. The cells were also reported to increase their metabolic activity and proliferation rate. An increase in cells number may be generated by both proliferation and migration [39, 56]. This finding was used to explain the role that fibrin plays in wound healing during the early repair stage by increasing cell proliferation to cover the wound [59]. Similar lack of collagen1 expression in fibroblasts cultured on PLGA nanofibers was demonstrated in mesenchymal stem cells seeded on PLGA scaffolds *in vivo* [60]. It has also been reported that, in 2D models, rounded cells proliferated at slower rates and expressed less collagen1 transcripts compared to spindle-shaped cells. At the same time, their MMP1 and MMP2 expression and activities were increased [61]. Fibronectin, which mediates a variety of cellular interactions with ECM via its active binding sites, was shown to be involved in human chondrocytes attachment and migration toward the PLGA scaffold. This unique role of fibronectin might explain its constant expression in cells attached to the coated and uncoated fibers in our model scaffolds. It is significant that this upregulated fibronectin gene expression without the production of collagen1, did not affect cartilage repair and regeneration [62]. Further expression profiling of additional fibroblastic markers, such as the alpha-smooth muscle actin (α -SMA), is recommended to determine the impact of the fibers on fibroblasts and ECM contractility [63, 64]. Overall, our findings support the previous claims that mechanical tension produced by collagen fibers on fibroblasts is required for the efficient synthesis of collagen [65]. Cells spread in the ECM environment are exposed to low-tension forces resulting in low synthesis and compaction of collagen matrix. However, when collagen fibers produce a sufficient mechanical tension on fibroblasts, collagen synthesis is elevated, and fibers compacted and aligned so that they parallel the principal strain in the collagen lattice. Once established, this stress effect may be

maintained at a constant level over long periods of time [53].

Cellular fusion is one of the fundamental processes taking place during tissue development and wound healing [19, 20]. In our scaffold model, fusion was present in the clustered cells developed within collagen nanofibers; a similar phenomenon was detected in collagen-based hydrogels [22].

5. Conclusion

This study demonstrates multi-functionality of the protein-coated PLGA airbrushed nanofiber platform (figure 8): (a) capability to attract gingival fibroblast monolayers and spheroids deposited on ECM hydrogel, (b) empowerment of fibroblast migration toward and within the nanofibers, and (c) arrangement of cells in conformations similar to either dense or loose connective tissues. Furthermore, fibroblasts within the coated nanofibers retained the vital tissue functions by expressing structural proteins such as collagen1 and fibronectin, and the ECM turnover enzyme MMP2. Employing gingival fibroblast spheroids as initial building blocks in conjunction with nanofiber scaffolds may be a more efficient way to initiate tissue regeneration than utilizing cell monolayers. Further investigations appear necessary to establish: (1) better control of the effect of fibrin nanofibers on the formation of loose connective tissue, (2) fibroblast interactions with the environmental components, such as macrophages and adipocytes, and (3) interactions of fibroblast-released growth factors with epithelial cells [66]. *in vivo* studies followed by histological analysis will provide essential information on cell distribution in each connective layer of the developing tissue. These future studies will provide an answer as to whether the proposed platform shows potential for regenerating other more complex organs (e.g. skin, heart, bone or spinal cord) in addition to gingiva.

Acknowledgments

This study was supported by the American Dental Association Foundation (ADAF). We would like to express our gratitude to Deborah Murphy-Marsh, and Wayne Garafola, from Sartorius for providing Sartocheck® 3 Plus equipment and training.

Disclosure statement

The authors indicate no potential conflicts of interest.

Disclaimer

Certain commercial materials and equipment are identified in this article to specify the experimental procedure. In no instance does such identification imply recommendation or endorsement by the ADA Foundation or that the material or equipment identified is necessarily the best available for the purpose.

ORCID iDs

Gili Kaufman  <https://orcid.org/0000-0002-6686-7710>

Xavier-Lewis Palmer  <https://orcid.org/0000-0002-1289-5302>

References

- [1] Nooh N and Graves DT 2003 Healing is delayed in oral compared to dermal excisional wounds *J. Periodontol.* **74** 242–6
- [2] Guo S and Dipietro LA 2010 Factors affecting wound healing *J. Dent. Res.* **89** 219–29
- [3] Kinikoglu B, Auxenfans C, Pierrillas P, Justin V, Breton P, Burillon C, Hasirci V and Damour O 2009 Reconstruction of a full-thickness collagen-based human oral mucosal equivalent *Biomaterials* **30** 6418–25
- [4] Cekici A, Kantarci A, Hasturk H and Van Dyke TE 2014 Inflammatory and immune pathways in the pathogenesis of periodontal disease *Periodontol 2000* **64** 57–80
- [5] Nishimura M, Takase K, Suehiro F and Murata H 2012 Candidates cell sources to regenerate alveolar bone from oral tissue *Int. J. Dent.* **2012** 1–5
- [6] Karring T, Lang NP and Löe H 1975 The role of gingival connective tissue in determining epithelial differentiation *J. Periodontol. Res.* **10** 1–11
- [7] Mackenzie IC and Hill MW 1984 Connective tissue influences on patterns of epithelial architecture and keratinization in skin and oral mucosa of the adult mouse *Cell Tissue Res.* **235** 551–9
- [8] Henrikson RC, Kaye GI and Mazurkiewicz JE 1997 The national medical series for independent study: histology *Oral Cavity* (Media, PA: Lippincott Williams and Wilkins) ch 22
- [9] Luitaud C, Laflamme C, Semlali A, Saidi S, Grenier G, Zakrzewski A and Rouabhia M 2007 Development of an engineering autologous palatal mucosa-like tissue for potential clinical applications *J. Biomed. Mater. Res. B Appl. Biomater.* **83** 554–61
- [10] Moharamzadeh K, Brook IM, Van Noort R, Scutt AM, Smith KG and Thornhill MH 2008 Development, optimization and characterization of a full-thickness tissue engineered human oral mucosal model for biological assessment of dental biomaterials *J. Mater. Sci., Mater. Med.* **19** 1793–801
- [11] Alaminos M, Garzón I, Sánchez-Quevedo MC, Moreu G, González-Andrades M, Fernández-Montoya A and Campos A 2007 Time-course study of histological and genetic patterns of differentiation in human engineered oral mucosa *J. Tissue Eng. Regen. Med.* **1** 350–9
- [12] Hotta T, Yokoo S, Terashi H and Komori T 2007 Clinical and histopathological analysis of healing process of intraoral reconstruction with *ex vivo* produced oral mucosa equivalent *Kobe J. Med. Sci.* **53** 1–14 (PMID: 17579297)
- [13] Alberts B, Johnson A, Lewis J, Raff M, Roberts K and Walter P 2002 Molecular biology of the cell *The Extracellular Matrix of Animals* (New York: Garland Science)
- [14] Herchenhan A, Bayer ML, Svensson RB, Magnusson SP and Kjaer M 2013 *In vitro* tendon tissue development from human fibroblasts demonstrates collagen fibril diameter growth associated with a rise in mechanical strength *Dev. Dyn.* **242** 2–8
- [15] Jiang H and Grinnell F 2005 Cell–matrix entanglement and mechanical anchorage of fibroblasts in three-dimensional collagen matrices *Mol. Biol. Cell.* **16** 5070–6
- [16] Eckes B, Zweers MC, Zhang ZG, Hallinger R, Mauch C, Aumailley M and Krieg T 2006 Mechanical tension and integrin alpha 2 beta 1 regulate fibroblast functions *J. Invest. Dermatol. Symp. Proc.* **11** 66–72
- [17] Asakura S et al 1997 Fibroblasts spread on immobilized fibrin monomer by mobilizing a beta1-class integrin, together with a vitronectin receptor alphavbeta3 on their surface *J. Biol. Chem.* **272** 8824–9

- [18] Yang W, Wu B, Asakura S, Kohno I and Matsuda M 2004 Soluble fibrin augments spreading of fibroblasts by providing RGD sequences of fibrinogen in soluble fibrin *Thromb Res.* **114** 293–300
- [19] Jakab K, Neagu A, Mironov V, Markwald R R and Forgacs G 2004 Engineering biological structures of prescribed shape using self-assembling multicellular systems *Proc. Natl Acad. Sci. USA* **101** 2864–9
- [20] Pérez-Pomares J M and Foty R A 2006 Tissue fusion and cell sorting in embryonic development and disease: biomedical implications *Bioessays* **28** 809–21
- [21] Ou K L and Hosseinkhani H 2014 Development of 3D *in vitro* technology for medical applications *Int. J. Mol. Sci.* **15** 17938–62
- [22] Kaufman G, Nunes L, Eftimiades A and Tutak W 2016 Enhancing 3D structure of adherent gingival fibroblasts and spheroids via fibrous protein-based hydrogel cover *Cells Tissues Organs.* **202** 343–54
- [23] Tutak W, Sarkar S, Lin-Gibson S, Farooque T M, Jyotsnendu G, Wang D, Kohn J, Bolikal D and Simon C G Jr 2013 The support of bone marrow stromal cell differentiation by airbrushed nanofiber scaffolds *Biomaterials* **34** 2389–98
- [24] Pham Q P, Sharma U and Mikos A G 2006 Electrospinning of polymeric nanofibers for tissue engineering applications: a review *Tissue Eng.* **12** 1197–211
- [25] Xu C Y, Inai R, Kotaki M and Ramakrishna S 2004 Aligned biodegradable nanofibrous structure: a potential scaffold for blood vessel engineering *Biomaterials* **25** 877–86
- [26] Xu C, Inai R, Kotaki M and Ramakrishna S 2004 Electrospun nanofiber fabrication as synthetic extracellular matrix and its potential for vascular tissue engineering *Tissue Eng.* **10** 1160–8
- [27] Wei Q, Becherer T, Angioletti-Uberti S, Dzubiella J, Wischke C, Neffe A T, Lendlein A, Ballauff M and Haag R 2014 Protein interactions with polymer coatings and biomaterials *Angew. Chem., Int. Ed. Engl.* **53** 8004–31
- [28] Nath N, Hyun J, Ma H and Chilkoti A 2004 Surface engineering strategies for control of protein and cell interactions *Surf. Sci.* **570** 98–110
- [29] Vasita R and Katti D S 2006 Nanofibers and their applications in tissue engineering *Int. J. Nanomedicine* **1** 15–30
- [30] Varghese M C, Balin A K, Carter D M and Caldwell D 1986 Local environment of chronic wounds under synthetic dressings *Arch. Dermatol.* **122** 52–7
- [31] Tandara A A and Mustoe T A 2004 Oxygen in wound healing —more than a nutrient *World J. Surg.* **28** 294–300
- [32] Rippon M, White R and Davies P 2007 Skin adhesives and their role in wound dressings *Wounds UK* **3** 76–86
- [33] Asti A and Gioglio L 2014 Natural and synthetic biodegradable polymers: different scaffolds for cell expansion and tissue formation *Int. J. Artif. Organs* **37** 187–205 (PMID:24744164)
- [34] Hotaling N A, Bharti K, Kriel H and Simon C G Jr 2015 DiameterJ: a validated open source nanofiber diameter measurement tool *Biomaterials* **61** 327–38
- [35] Buskermolen J K, Reijnders C M, Spiekstra S W, Steinberg T, Kleverlaan C J, Feilzer A J, Bakker A D and Gibbs S 2016 Development of a full-thickness human gingiva equivalent constructed from immortalized keratinocytes and fibroblasts *Tissue Eng. Part C Methods* **22** 781–91
- [36] Colley H E, Hearnden V, Jones A V, Weinreb P H, Violette S M, Macneil S, Thornhill M H and Murdoch C 2011 Development of tissue-engineered models of oral dysplasia and early invasive oral squamous cell carcinoma *Br. J. Cancer* **105** 1582–92
- [37] Wei K and Kim I-S 2013 Advances in nanofibers *Fabrication of Nanofibrous Scaffolds by Electrospinning* (Rijeka: InTech) pp 103–24
- [38] Behrens A M, Kim J, Hotaling N, Seppala J E, Kofinas P and Tutak W 2016 Rapid fabrication of poly(DL-lactide) nanofiber scaffolds with tunable degradation for tissue engineering applications by air-brushing *Biomed. Mater.* **11** 1–17
- [39] Bacakova M, Musilkova J, Riedel T, Stranska D, Brynda E, Zaloudkova M and Bacakova L 2016 The potential applications of fibrin-coated electrospun polylactide nanofibers in skin tissue engineering *Int. J. Nanomedicine* **11** 771–89
- [40] Ma P X 2008 Biomimetic materials for tissue engineering *Adv. Drug. Deliv. Rev.* **60** 184–98
- [41] Wang X, Ding B and Li B 2013 Biomimetic electrospun nanofibrous structures for tissue engineering *Mater Today* **6** 229–41
- [42] Anseth K S, Bowman C N and Brannon-Peppas L 1996 Mechanical properties of hydrogels and their experimental determination *Biomaterials* **17** 1647–57
- [43] Naficy S, Kawakami S, Sadeghovaad S, Wakisaka M and Spinks G M 2013 Mechanical properties of interpenetrating polymer network hydrogels based on hybrid ionically and covalently crosslinked networks *J. Appl. Polym. Sci.* **130** 2504–13
- [44] Jaspers M, Pape A C, Voets I K, Rowan A E, Portale G and Kouwer P H 2016 Bundle formation in biomimetic hydrogels *Biomacromolecules* **17** 2642–9
- [45] Gentile P, Chiono V, Carmagnola I and Hatton P V 2014 An overview of poly(lactic-co-glycolic) acid (PLGA)-based biomaterials for bone tissue engineering *Int. J. Mol. Sci.* **15** 3640–59
- [46] Zhang Y Z, Su B, Venugopal J, Ramakrishna S and Lim C T 2007 Biomimetic and bioactive nanofibrous scaffolds from electrospun composite nanofibers *Int. J. Nanomedicine* **2** 623–38
- [47] Hotaling N A, Bharti K, Kriel H and Simon C G 2015 Dataset for the validation and use of DiameterJ: an open source nanofiber diameter measurement tool *Data in Brief* **5** 13–22
- [48] Tutak W, Gelven G, Markle C and Palmer X L 2015 Rapid polymer fiber airbrushing: impact of a device design on the fiber fabrication and matrix quality *J. Appl. Polym. Sci.* **132** 42813
- [49] Refojo M F 1965 Permeation of water through some hydrogels *J. Appl. Polym. Sci.* **9** 3417–26
- [50] Everett D H 2007 *Basic Principles of Colloid Science* 1st edn (London: Royal Society of Chemistry)
- [51] Lück M, Karin-Frauke P, You-Xin L, Torsten B, Rainer H M and Kissel T 1998 Plasma protein adsorption on biodegradable microspheres consisting of poly (D, L-lactide-co-glycolide), poly (L-lactide) or ABA triblock copolymers containing poly (oxyethylene): influence of production method and polymer composition *Journal of Controlled Release* **55** 107–20
- [52] Arima Y and Hiroo I 2007 Effect of wettability and surface functional groups on protein adsorption and cell adhesion using well-defined mixed self-assembled monolayers *Biomaterials* **28** 3074–82
- [53] Tomasek J J, Gabbiani G, Hinz B, Chaponnier C and Brown R A 2002 Myofibroblasts and mechano-regulation of connective tissue remodelling *Nat. Rev. Mol. Cell Biol.* **3** 349–63
- [54] Barker D A, Bowers D T, Hughley B, Chance E W, Klembczyk K J, Brayman K L, Park S S and Botchwey E A 2013 Multilayer cell-seeded polymer nanofiber constructs for soft-tissue reconstruction *JAMA Otolaryngol Head Neck Surg.* **139** 914–22
- [55] Laurens N, Koolwijk P and de Maat M P 2006 Fibrin structure and wound healing *J. Thromb Haemost.* **4** 932–9
- [56] Bacakova M, Pajorova J, Stranska D, Hadraba D, Lopot F, Riedel T, Brynda E, Zaloudkova M and Bacakova L 2017 Protein nanocoatings on synthetic polymeric nanofibrous membranes designed as carriers for skin cells *Int. J. Nanomedicine* **12** 1143–60
- [57] Zhang W, Lavine K J, Epelman S, Evans S A, Weinheimer C J, Barger P M and Mann D L 2015 Necrotic myocardial cells release damage-associated molecular patterns that provoke fibroblast activation *in vitro* and trigger myocardial inflammation and fibrosis *in vivo* *J. Am. Heart Assoc.* **4** 1–19
- [58] Vavken P, Joshi S M and Murray M M 2011 Fibrin concentration affects ACL fibroblast proliferation and collagen synthesis *Knee* **18** 42–6
- [59] McCulloch J M and Kloth L C 2010 Wound healing evidence-based management *The Wound Healing Process* 4th edn (Philadelphia, PA: F A Davis Company) ch 2

- [60] Park J S and Park K H 2016 Light enhanced bone regeneration in an athymic nude mouse implanted with mesenchymal stem cells embedded in PLGA microspheres *Biomater. Res.* **20** 1–8
- [61] Chen X and Thibeault S L 2012 Response of fibroblasts to transforming growth factor- β 1 on two-dimensional and in three-dimensional hyaluronan hydrogels *Tissue Eng. Part A* **18** 2528–38
- [62] Foldager C B, Bunger C, Nielsen A B, Ulrich-Vinther M, Munir S, Everland H and Lind M 2012 Dermatan sulphate in methoxy polyethylene glycol-poly(lactide-co-glycolic acid) scaffolds upregulates fibronectin gene expression but has no effect on *in vivo* osteochondral repair *Int. Orthop.* **36** 1507–13
- [63] Hinz B, Celetta G, Tomasek J J, Gabbiani G and Chaponnier C 2001 Alpha-smooth muscle actin expression upregulates fibroblast contractile activity *Mol. Biol. Cell* **12** 2730–41
- [64] Jester J V and Ho-Chang J 2003 Modulation of cultured corneal keratocyte phenotype by growth factors/cytokines control *in vitro* contractility and extracellular matrix contraction *Exp. Eye Res.* **77** 581–92
- [65] Varani J, Dame M K, Rittie L, Fligiel S E, Kang S, Fisher G J and Voorhees J J 2006 Decreased collagen production in chronologically aged skin *Am. J. Pathol.* **168** 1861–8
- [66] ohlund D, Elyada E and Tuveson D 2014 Fibroblast heterogeneity in the cancer wound *J. Exp. Med.* **211** 1503–23